ELSEVIER

Polymer 41 (2000) 4249–4266

polymer

Relations between spinning, molecular structure and end-use properties of polyethylene naphthalate tyre yarns

C.J.M. van den Heuvel[a,*], E.A. Klop[b]

[a]*Acordis Research Arnhem, Velperweg 76, P.O. Box 9600, 6800 TC Arnhem, The Netherlands*
[b]*Akzo Nobel Research Arnhem, Velperweg 76, P.O. Box 9300, 6800 SB Arnhem, The Netherlands*

Received 18 March 1999; received in revised form 6 July 1999; accepted 30 July 1999

Abstract

Characteristic features of the molecular structure of polyethylene naphthalate (PEN) are the rigidity of the polymer chains and the occurrence of two *trans* conformations of the naphthalene ring, the so-called α- and β-conformations. The rigidity of the molecular chains permits production of PEN tyre yarns by a simple high-speed melt spinning process without drawing steps. The yarns crystallize with the naphthalene ring in the β-conformation. The crystal structure of this modification (PEN-β) is monoclinic (spacegroup P 1 2_1/a 1) with unit cell parameters $a = 9.49$, $b = 13.31$, $c = 12.61$ Å, $\alpha = 90$, $\beta = 135$, $\gamma = 90°$. The melting points of the β-crystals can be over 300°C. Under the influence of stress, as occurs for instance when the yarns are dipped for application in tyres, the crystals transform irreversibly into the fully extended α-form with retention of a high melting point. The ultimate modulus of PEN yarns produced by different processes is substantially higher than that of polyethylene terephthalate. However, in the amorphous domains of PEN yarns, rotation of the naphthalene ring induces conformational α ⇔ β and *cis* ⇔ *cis* transitions which negatively influence the dynamic properties. More specifically, the work loss is four times as high as that of other tyre yarns, and, going from 20 to 60°C, i.e. a moderate in-use temperature for tyres, the dynamic modulus decreases by 20%.

Keywords: Polyethylene naphthalate; Molecular structure; Spinning

1. Introduction

Polyethylene naphthalate (PEN) is a high-performance, high-priced polymer with opportunities in several markets, including packaging, films, and fibers. In the case of packaging, use is made of PEN's good barrier properties and high glass transition temperature, making the polymer suitable for applications such as cans for drinks and hot-filled bottles. Compared to polyethylene terephthalate (PET), PEN has a higher modulus, which may be advantageous in films, e.g. for advanced photo system cameras and in industrial fiber applications.

The properties of PEN have been described in a number of publications (cf. Refs. [1–23] and references cited therein). This article concerns the relations between spinning, physical structure, and mechanical properties of PEN yarns, with a focus on high-melting yarns obtained using a relatively simple spinning process recently developed by us [24]. Two general aspects of PEN's molecular structure are discussed, namely the rigidity of the polymer chains and the occurrence of the so-called *trans* α- and β-conformations of the naphthalene rings in the crystalline and amorphous domains. Their influence on the stress–strain and dynamic behavior of the yarns will be considered extensively.

2. Experimental

2.1. Polymerization

PEN oligomer was produced by transesterification of dimethyl-2,6-naphthalenedicarboxylate and ethylene glycol at 230°C using manganese diacetate as catalyst. Subsequently, the oligomer was polymerized at 290°C with an antimony trioxide catalyst. Postcondensation of the chips to high molecular weight PEN was carried out in the solid state by heating the chips for 14 h under high vacuum at 227°C in a tumble dryer. By the above procedure, PEN chips with a melt flow index (MFI) of 18.6 g/10 min. were prepared. For more details see Ref. [17].

* Corresponding author. Tel.: +31-26-3662220; fax: +31-26-3663009.
E-mail address: jurriaan.vandenheuvel@research-ahm.acordis.com (C.J.M. van den Heuvel).

0032-3861/00/$ - see front matter
PII: S0032-3861(99)00554-6

Table 1
Process conditions, mechanical properties and physical structure of PEN yarns, spun at high speed, and with low and high draw-down, respectively

Spinning speed (m/min)	4000	4000
Spinning temperature (°C)	312	312
Spinneret hole diameter (μm)	400	1000
Throughput per spinneret hole (g/min)	2.4	1.1
Extrusion velocity (m/min)	16.5	1.2
Draw-down	*243*	*3336*
Shear rate (1/s)	5495	160
Maximum inertial stress (cN/tex)	0.44	0.44
Maximum air drag (a.u.)	61	124
MFI (g/10min)	18.6	18.6
Filament diameter (μm)	25.3	18.4
Elongation at rupture (%)	19.6	9.7
Breaking tenacity (mN/tex)	369	590
Modulus TASE5% (mN/tex)	221	324
Shrinkage SHA190 (%)	19.2	1.3
Polymorphic form of crystal	–	β
Apparent crystal thickness Λ120 (Å)	–	57
Density (kg/m^3)	1349.1	1355.5
Apparent crystallinity	0.25	0.32
Melting point (°C)	270	298
Birefringence	0.2357	0.1885
Sonic modulus (GPa)	18.6	24.7

2.2. Spinning

The spinning machine comprised an electrically heated 30 mm extruder and a metering pump to adjust the polymer mass flow. The spinning assembly contained filters and a spinneret with 36 circular holes. The temperature of the extruder, metering pump and spinning assembly was maintained at 310°C. The yarn was cooled with ambient air. The winding speed was 4000 m/min. For further details see Table 1 and Ref. [17].

2.3. Drawing

Cold drawing was carried out by loading a piece of yarn for 10 min. The length was measured, before and after the loading, at a tension of 2 cN/tex to enable calculation of the draw ratio. For hot drawing, the yarn was transported over godets in approximately 8 s through a tubular oven with a length of 120 cm and a parabolic temperature profile ranging from 180° at the ends to 280°C in the middle. The draw ratio was calculated from the speeds of the godets.

2.4. Stress–strain curves of the yarns

Mechanical testing was carried out on an Instron tensile tester, applying a gauge length of 500 mm, a pretension of 5 mN/tex, and a clamp speed of 500 mm/min. The yarns were twisted 60 turns per meter. For details see Ref. [17]. Characteristic mechanical properties derived from the stress–strain curves are the maximum tenacity (breaking tenacity), the tenacity at specified elongation of 2 and 5% (TASE2 and TASE5), and the elongation at rupture, which is the point where the stress is 5% lower than the maximum stress.

2.5. Shrinkage

The hot-air shrinkage (SHA190) was calculated from the decrease of length of skeins when tensionless heated in hot air at 190°C for 15 min (cf. Ref. [17]).

2.6. Stress-controlled cyclic loading

For a detailed description of the method see Ref. [25].

2.7. Strain-controlled dynamic mechanical analysis

Dynamic mechanical tests were carried out in the extension mode of a Qualimeter Eplexor at a frequency of 10 Hz. The temperature dependence of the complex modulus was measured over a range from −150 to 250°C with intervals of 40°C using an intermediate hold force of 5 mN/tex and a heating rate of 1°C/min. During each measurement, a static strain of 0.5% and a dynamic strain of 0.05% were applied. The actual gauge length was used to calculate the required static and dynamic elongations (initial gauge length 40 mm).

2.8. Melt flow index

The MFI of the polymer equals the mass flow per minute through a nozzle channel of 2.1 mm in diameter under a load of 2160 g at 310°C. For a detailed description of the method see Ref. [24].

2.9. Wide angle X-ray scattering

Wide angle X-ray scattering (WAXS) measurements were carried out using a Philips PW1050 transmission diffractometer equipped with a quartz curved crystal monochromator. Samples were prepared by winding a smooth layer of yarn filaments around a metal frame. The X-ray scans were fitted by means of Pearson functions (Ref. [26]). The measurements at elevated temperatures were performed using a Siemens D5000 diffractometer with a HTK10 hot stage. Flat plate photographs were recorded by employing a Statton camera with graphite monochromator. In the XRD measurements Cu K_α radiation was used.

2.10. Density

The density of the yarns was determined at 23° in a Davenport gradient column containing *n*-heptane and tetrachloromethane mixed in a ratio gradually decreasing in the downward direction (cf. Ref. [17]).

2.11. Birefringence

The birefringence was determined on filaments, immersed in dibutyl phthalate and placed at an angle of 45° relative to the crossed polarizers of a microscope,

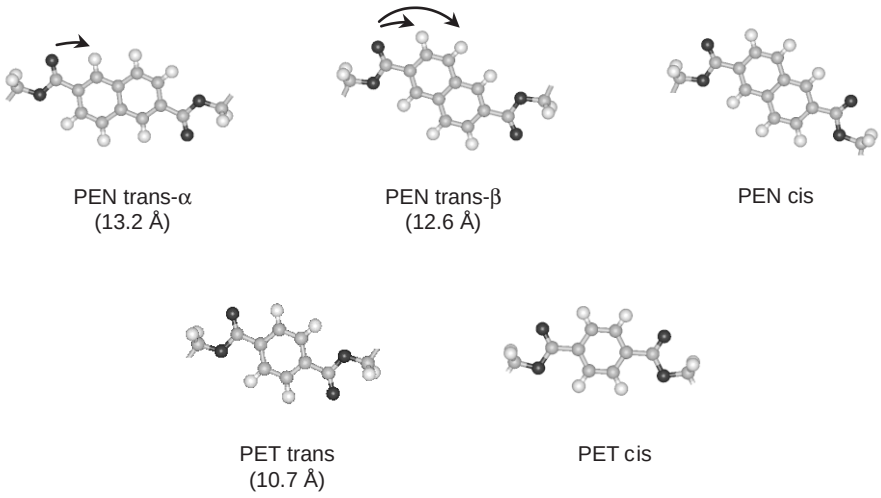

Fig. 1. Conformations of aromatic rings in PEN and PET.

equipped with a sodium lamp ($\lambda = 0.5893$ μm) and a De Sénarmont compensator (cf. Ref. [17]).

2.12. Sonic modulus

A yarn sample was clamped at one end, passed horizontally over a couple of pulleys, and loaded at the other end with 2 cN/tex. Between the pulleys, two piezo-electric transducers were placed on the yarn for transmitting and receiving sonic pulses of 60 μs with a frequency of 10 kHz (see also Ref. [17]). The product of the density and the square of the sound velocity equals the sonic modulus of the yarn.

2.13. Melting point

The melting points were determined with a Perkin–Elmer DSC-7 differential scanning calorimeter calibrated with indium (melting point 156.6°C) and zinc (melting point 419.5°C). A cup with 2.5 mg of a yarn sample was heated at a rate of 20°C/min and the difference in heat flow between this cup and an empty reference cup was recorded as a thermogram.

2.14. Molecular calculations

Conformational energies of model compounds were calculated with the aid of the Insight/Discover molecular mechanics package V.3.0.0 [27] using the PCFF force field, a force field especially developed for polymers. Model building and simulation of diffraction patterns were performed using the CERIUS2 software of molecular simulations.

3. Molecular structure

In Section 1, two characteristic features of PEN were mentioned, namely the rigidity of the polymer chains and the occurrence of two *trans* conformations of the ring. These aspects of PEN will be discussed here in more detail.

3.1. Chain rigidity

Owing to the larger size of the aromatic ring system in semi-crystalline PEN, the number of flexible ethylene glycol groups is about 23% lower than in PET. Therefore, the modulus of an extended PEN molecule is expected to be higher, despite the fact that in the case of PEN, measured in cross section, the number of polymer chains is about 8% lower than for PET. Indeed, by means of WAXS, Nakamae et al. [13,15]) measured elastic moduli of 145 and 108 GPa for PEN-α and PET crystals, respectively. The Young's modulus of a yarn not only depends on the molecular chain rigidity, but also on the orientation and shear modulus [28], which depend in turn on molecular interactions, chain conformations, crystallinity, etc. In practice, the Young's modulus of drawn PEN yarn proves to be substantially higher than that of PET [17].

In line with the observed higher chain rigidity, Jackson et al. measured relaxation times of $\approx 10^{-2}$ s at 300°C for PEN and $\approx 10^{-3}$ s at 275°C for PET [3]. During melt-spinning, the residence time of the polymer in the zone where the physical structure is formed, is in the order of $\approx 10^{-2}$ s. Therefore, it is not surprising that, in the case of PEN, the structure formation in terms of orientation [17] and orientation-induced crystallization proceeds more easily.

3.2. Molecular conformations

In PEN, there are two *trans* conformations of the naphthalene ring as a result of the absence of a twofold rotation axis through the $C_{aliphatic}$–$C_{aromatic}$ bonds of the ring system (Fig. 1). Note that such an axis is present in the case of PET, for which there is only one *trans* conformation. The two *trans*

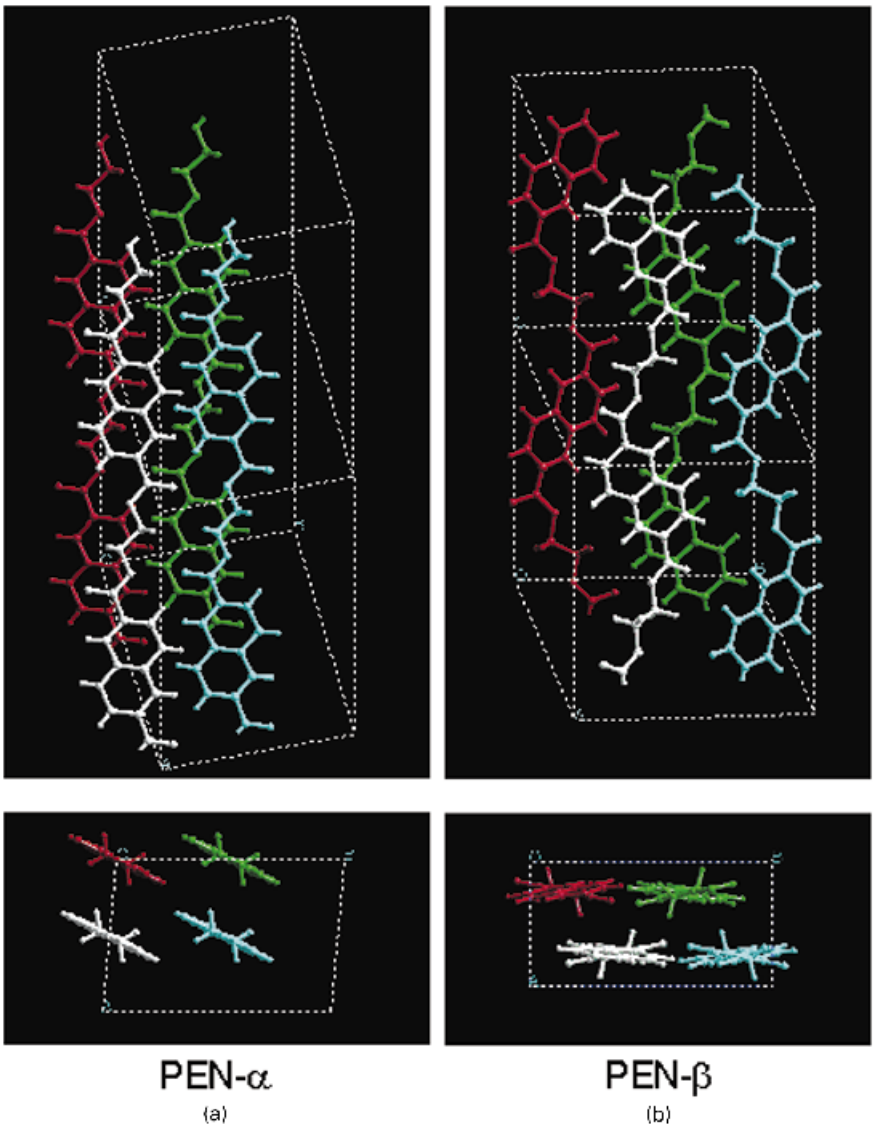

Fig. 2. (a) Crystal structure of PEN-α. The structure has extended chains with 1 chain per unit cell. Crystallographic data: triclinic, $P\bar{1}$, $a = 6.51$, $b = 5.75$, $c = 13.2$ Å, $\alpha = 81$, $\beta = 144$, $\gamma = 100°$, $\rho_c = 1.407$ g/cm^3. The *a* and *b*-axes are drawn twice as large for easy comparison with PEN-β. (b) Crystal structure of PEN-β. The structure has sinusoidal chains with 4 chains per unit cell. Crystallographic data: monoclinic, $P12_1/a1$, $a = 9.49$, $b = 13.31$, $c = 12.61$ Å, $\alpha = 90$, $\beta = 135$, $\gamma = 90°$, $\rho_c = 1.425$ g/cm^3.

conformations in PEN can be distinguished by the number of hydrogen atoms at the aromatic ring adjacent to the carbonyl oxygen atom. In the case of the *trans* α-conformation there is one such hydrogen, and in the case of the *trans* β-conformation there are two (see Fig. 1). Monomer units containing the α-conformation are almost 5% longer than those having the more sinusoidal β-conformation (lengths 13.2 and 12.6 Å, respectively). The aromatic ring system in both PEN and PET has only one *cis*-conformation (Fig. 1).

Owing to the rotation axis through the $C_{aliphatic}$–$C_{aromatic}$ bonds, the phenyl group rotates more easily than the naphthalene ring. What this means for the yarn properties, especially the dynamic properties, will be discussed later on.

3.3. α- and β-conformations in crystals

In the PEN-α crystal structure described by Mencik [2], the polymer molecules display the α-conformation (Fig. 2). This crystal structure resembles that of PET (Fig. 3) as regards the extended all-*trans* conformation of the chains and the type of unit cell (triclinic; one chain per unit cell). A second crystal structure was mentioned in a patent [1] and was also observed by Zachmann et al. [4] using synchrotron radiation. This polymorphic modification was designated as PEN-β by Buchner et al. [11] in their study of the kinetics of crystallization and melting of PEN. According to these authors the PEN-β crystal structure is triclinic with a four-chain unit cell containing polymer molecules which

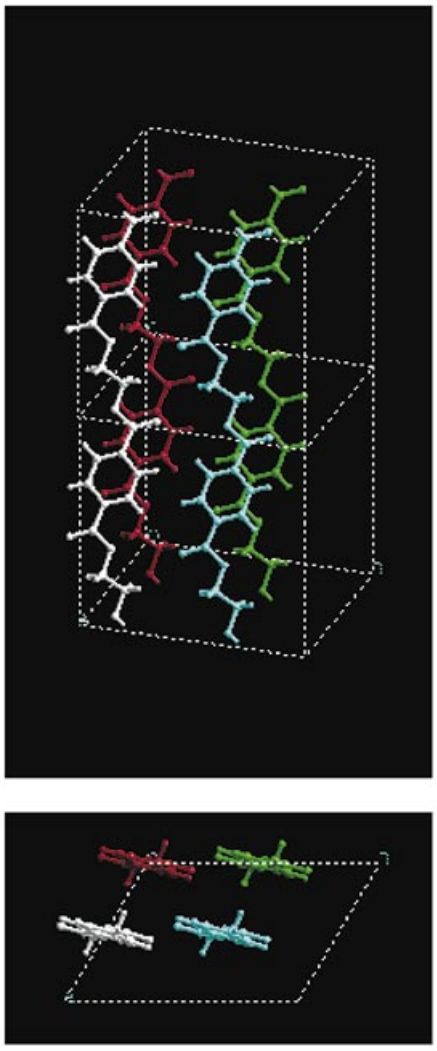

Fig. 3. Crystal structure of PET. The structure has extended chains with 1 chain per unit cell. Crystallographic data: triclinic, $P\bar{1}$, $a = 4.49$, $b = 5.88$, $c = 10.72$ Å, $\alpha = 100$, $\beta = 118$, $\gamma = 111°$, $\rho_c = 1.500$ g/cm^3 (Ref. [31]). The *a* and *b*-axes are drawn twice as large for easy comparison with PEN-β.

crystallize in the β-conformation. Unit cell parameters were reported, but a crystal structure was not presented.

By the high-speed spinning process outlined in the sequel, we obtained yarns containing β-crystals of very high perfection. The diffraction data of these fibers (Fig. 4) enabled us to determine the PEN-β structure. This structure is monoclinic with symmetry P 1 2_1/a 1 and unit cell parameters $a = 9.49$, $b = 13.31$, $c = 12.61$ Å, $\alpha = 90$, $\beta = 135$, $\gamma = 90°$ (which differ from those of Zachman et al. [4]). Fig. 2 displays the crystal structure; its fractional coordinates are listed in Table 2. The structure is characterized by a sinusoidal conformation of the polymer chains as shown in Fig. 2. Its structure determination will be reported in a forthcoming article [29].

Recently Liu et al. [30] proposed a model for the PEN-β crystal structure based on electron diffraction data (i.e. the [001] and [$\bar{1}$02] zones) of thin-film melt-crystallized material. The proposed model differs from that in Fig. 2 of the present report based on fiber diffraction data. Although the unit cell parameters do not differ much, Liu et al. report a different symmetry (viz. P 2_1/n 1 1) and hence a different packing of molecules in the unit cell. Here we note that the PEN-β structure as described in this report not only explains the fiber diffraction pattern shown in Fig. 4 but also explains the PEN-β electron diffraction patterns observed by Liu et al. This can be verified, e.g. by comparing the electron diffraction pattern shown in Fig. 5, simulated on the basis of the structure described in Table 2, with the electron diffraction pattern in Fig. 6b of Liu et al.

In practice, the α and β crystalline modifications can be easily recognized from their WAXS patterns (Fig. 4).

3.4. α- and β-conformations in amorphous domains

Like PET, PEN is a semi-crystalline material. Based on the crystalline densities and the isotropic amorphous density (see below), the volume fraction of crystalline material in steam-drawn PEN yarn, which contains α-crystals only, was found to be similar to that of PET i.e. ≈0.4 [17]. For better insight into the structure of amorphous PEN, an almost isotropic amorphous yarn was prepared by low-speed spinning (density $\rho = 1326.9$ kg/m^3, birefringence $\Delta n = 0.0047$). By drawing this yarn at 138°C with a draw ratio of 2.8, an anisotropic amorphous material was obtained (density $\rho = 1343.0$ kg/m^3, birefringence $\Delta n = 0.1880$). It is noted that the amorphous density increases with the orientation because of improved molecular packing and the formation of associates, which precede the formation of crystals. Actually, for calculation of crystalline and amorphous volumes, this effect should be taken into account (Ref. [31]; see also Refs. [5–10] as for the occurrence of rigid amorphous fractions).

The equatorial WAXS scans of both the above-mentioned amorphous samples do not simply show a smooth halo and are quite different (Fig. 6). Clearly, the scattering intensity in the 22–26° (2θ) range increases upon drawing. Note that the diffraction patterns of both the α and β crystalline modifications show peaks in this region, suggesting that the increase of intensity upon drawing is due to an increase in the amount of *trans* α- and β-conformations. This increase may arise from the transition of non-extended *cis* conformation into the more extended β-conformation and the fully extended α-conformation (Fig. 1). The latter conformations allow a higher degree of molecular ordering and orientation. The increase in the degree of molecular orientation is indicated by the increase in birefringence.

Before discussing the influence that α- and β-conformations

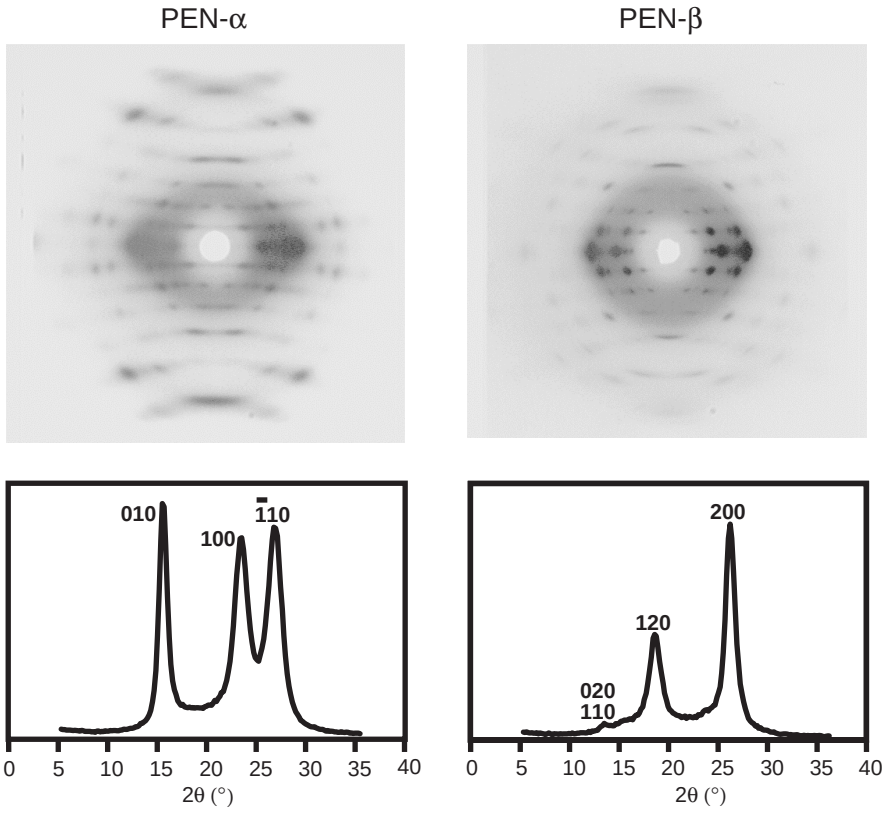

Fig. 4. Flat plate diffraction patterns (top) and equatorial scans (bottom) of semi-crystalline PEN yarns.

have on the mechanical properties, the behavior of PEN during high-speed spinning will be considered.

4. High-speed spun PEN yarns

4.1. The spinning process

From a molecular point of view, fiber production is polymer shaping by orientation and crystallization. During high-speed spinning of PET, a substantial part of the orientation and some crystallization takes place during the spinning step, although subsequent drawing steps are necessary for bringing orientation and crystallization at a level that give industrial yarns the required mechanical properties. As discussed above, PEN molecules are quite highly oriented during high-speed spinning. This posed the question whether it is possible to orient PEN to such an extent that drawing can be omitted. Such a one-step "draw spinning" process is interesting from an economical point of view.

In this context, it is worth noting that for PET, spinline orientation and crystallization are not only favored by a high-speed (high stress), but also to some extent by a high draw-down (= ratio of spinning hole area to cross section of the as-spun filament or ratio of winding to extrusion speed). A high draw-down enhances the thinning of the filament at the top of the spinline and therewith the acceleration of the spinning mass dV_x/dx and the inertial stress $\sigma_{\text{inertia}} = \rho V_x(V_x - V_0)$ (note: $R_x^2 V_x = W/(\pi\rho) =$ constant, where R_x is the radius of the filament at position x along the spinline, V_x is the spinning speed and W the mass throughput). In this part of the spinline, the inertial stress is the most dominant stress component [32], which together with the cooling rate, is fundamental to the formation of the physical structure during spinning.

The effect of draw-down in the case of high-speed spinning of PEN is illustrated here on the basis of two experiments, which are summarized in Table 1. In the first experiment, PEN was spun at a high speed but low draw-down, in the second experiment at high speed and high draw-down. To that end, different mass flow rates and spinning holes with different diameters were applied, as we observed for PET that orientation, crystallinity and crystal size increase when the spinning hole diameter is increased and the mass flow is reduced [33].

It is noted that the mass flow rate also influences the cooling of spinning filaments. So, on reducing the mass flow rate by a factor 2, the distance for cooling along the spinline is roughly halved.

4.2. Yarn properties

From the data in Table 1, it follows that the two high-speed

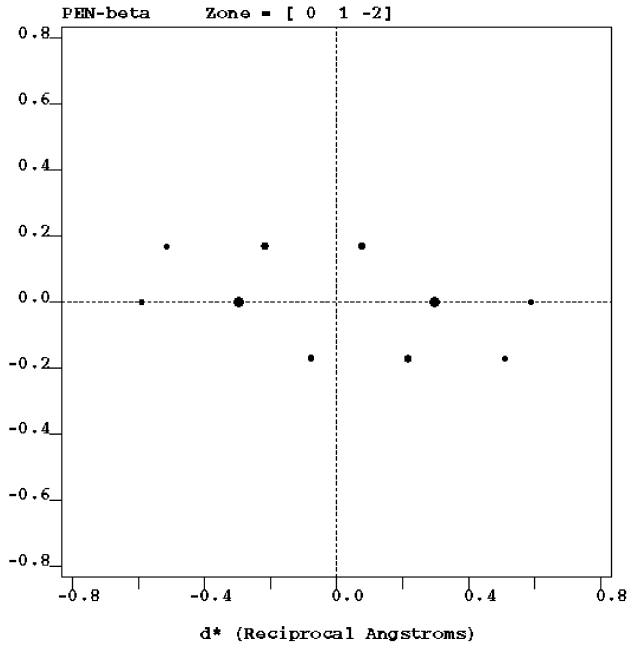

Fig. 5. CERIUS2 simulation of the [01$\bar{2}$] electron diffraction pattern of the PEN-β structure shown in Fig. 2.

Table 2
Fractional atomic coordinates of PEN-β based on fiber diffraction data. The coordinates of the complete unit cell contents are obtained by applying the symmetry operations -*x*, −*y*, −*z*; $\frac{1}{2}-x$, $\frac{1}{2}+y$, −*z* and $\frac{1}{2}+x$, $\frac{1}{2}-y$, *z* associated with P 2_1/a symmetry

Atom	*x*	*y*	*z*
C1	0.776	0.309	0.251
C2	0.781	0.251	0.069
C3	0.759	0.273	0.949
C4	0.780	0.371	0.925
C5	0.764	0.394	0.808
C6	0.693	0.220	0.730
C7	0.716	0.197	0.851
C8	0.713	0.406	0.269
C9	0.700	0.462	0.447
C10	0.722	0.439	0.567
C11	0.702	0.341	0.592
C12	0.719	0.318	0.709
C13	0.790	0.492	0.786
C14	0.767	0.515	0.666
O1	0.759	0.323	0.130
O2	0.818	0.164	0.119
O3	0.724	0.390	0.387
O4	0.661	0.549	0.397
H1	0.680	0.249	0.222
H2	0.927	0.291	0.359
H3	0.811	0.465	0.303
H4	0.563	0.426	0.160
H5	0.700	0.125	0.865
H6	0.826	0.548	0.857
H7	0.785	0.587	0.653
H8	0.675	0.285	0.524
H9	0.808	0.427	0.993
H10	0.656	0.164	0.658

PEN yarns are very different as to their physical structure and mechanical properties. The second yarn, spun at a high draw-down, has a higher breaking tenacity, higher modulus, and lower elongation at break. Actually, as shown further on, the yarn is suited for use as tyre yarn. There is no necessity for additional drawing steps, as required for more conventional processes. So, it is possible indeed to produce PEN tyre yarn by a one-step process.

A remarkable feature of the "high draw-down" yarn is the plateau in its stress–strain curve, the origin of which will be discussed later. The yarn contains well-developed β-crystals (Fig. 7) with a melting point of no less than 298°C! (Table 1; melting points as high as 307°C have been obtained by draw spinning). Apparently, orientation-induced crystallization has occurred just below the spinning temperature of 310°C. As discussed above, the high draw-down effects the build-up of the stress in the top of the spinline, so that the prerequisite for orientation-induced crystallization, namely high stress at high temperature, is

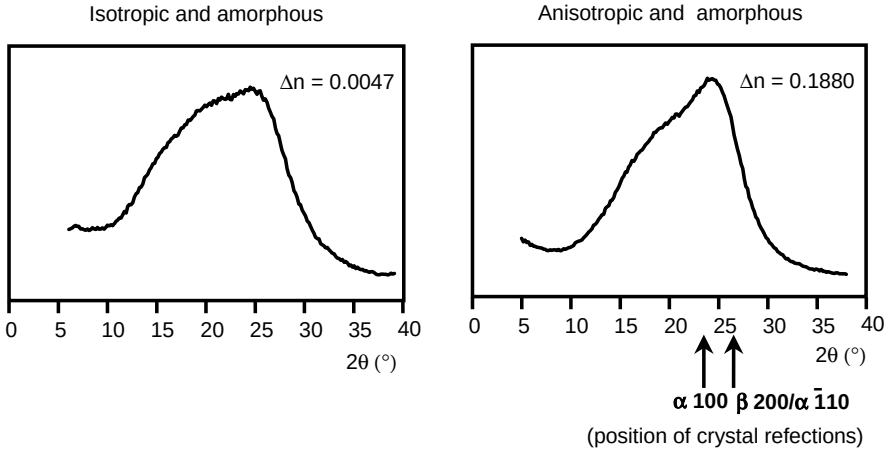

Fig. 6. Equatorial WAXS scans of amorphous PEN yarn before (left) and after drawing at 135°C (right).

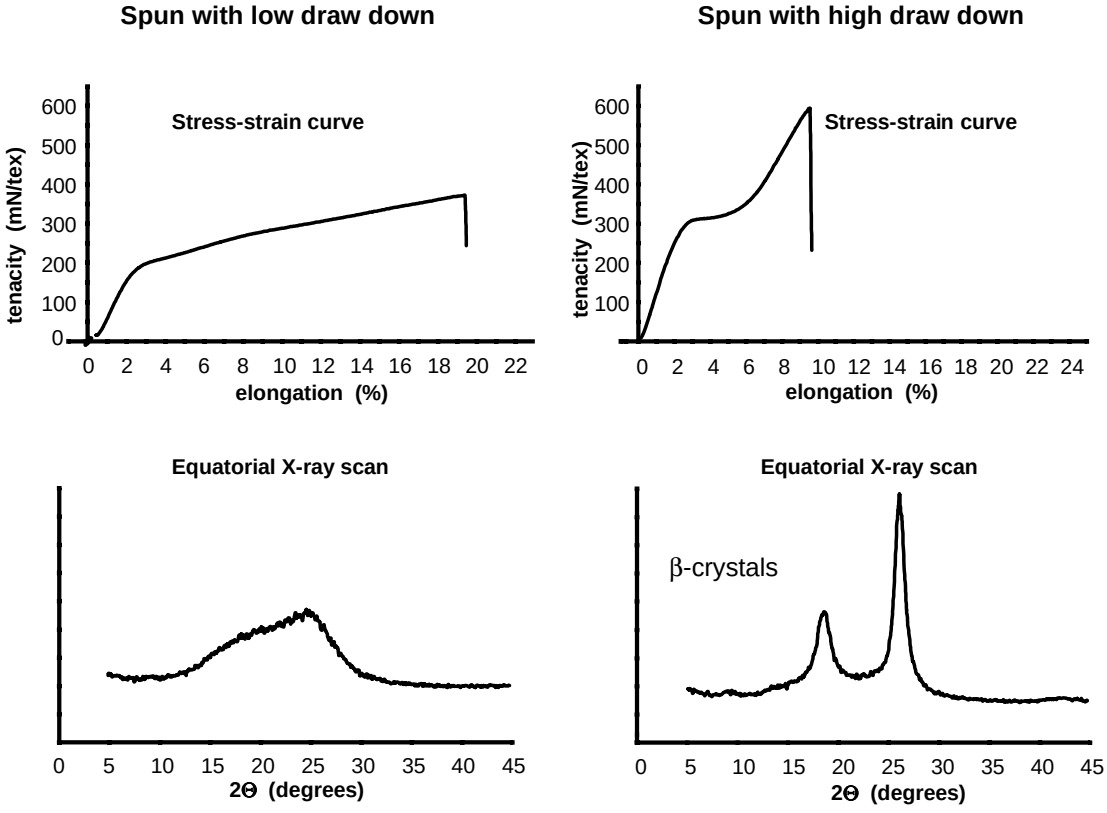

Fig. 7. Stress–strain curves and equatorial WAXS scans of PEN yarns spun at 4000 m/min.

fulfilled (cf. Ref. [34]). Under such circumstances, especially long stiff molecules with long relaxation times easily align and form crystals. Compared with lamellar crystallization, the decrease in entropy during orientation-induced crystallization is smaller and the presence of fewer chain folds implies a larger enthalpy change so that the melting point will be higher. Usually, the melting point of semi-crystalline PEN ranges from 265 to 270°C.

It is somewhat surprising that the orientation (*stress*) induced crystals are of the *sinusoidal* β-type instead of the *extended* α-type. Actually, it is generally observed for PEN that at temperatures above 220°C there is an increasing tendency for both thermally and orientation induced crystals to be formed in the polymorphic β-form [11,12,20,21,23]. Possibly, in the amorphous regions at these temperatures, there is a predominance of the entropically favored β-conformations.

Miyata et al. [21] have spun PEN at high speeds (5000–9000 m/min) with a high yield (5 g/min) through a single spinning hole with a diameter of 1 mm. Yarns were obtained with melting peaks ranging from 275 to 293°C. The soldification (necking) temperature during spinning ranged from 135 to 180°C. This indicates that crystals are formed within a wide temperature range, possibly for a large part by thermal crystallization. Comparing their WAXS equator scans with our scan as displayed in the right-hand side of Fig. 7, it can be concluded that the crystalline perfection of the material in this study is considerably higher.

Another point to discuss is the fact that the birefringence (Δn) of the second yarn, spun at a high draw-down, is much lower than that of the first yarn (see Table 1). At first sight, one might come to the conclusion that the second yarn has a lower molecular orientation. However, this seems in conflict with the presence of well-oriented β-crystals and the observed mechanical properties. There must be another reason. On considering the spatial ordering of the β-crystals (Fig. 2), it can be seen that in a monomer unit, the cloud of π-electrons of the aromatic ring, which contribute substantially to the polarizability, makes an angle of about 42° with the chain axis, whereas in the case of the α-crystals this angle is about 8°. Further, $\Delta n = \Delta n_{\max}\langle P_2\rangle$ wherein the second moment of the orientation distribution $\langle P_2\rangle = (3\langle\cos^2\theta\rangle - 1)/2$ with θ the angle between the chain axis and the yarn. Based on the different position of the π-electrons, it may be expected that $\Delta n_{\max}$ of the β-crystals is three times smaller than that of the α-crystals. Of course the position of the conjugated carbonyl groups and the packing density also play a part. Nevertheless, it seems reasonable to suppose that $\Delta n_{\max}$ of the β-crystals is considerably lower than that of the α-crystals. So, the occurrence of α- and β-conformations in amorphous and crystalline domains complicates the use of birefringence as a measure for the orientation.

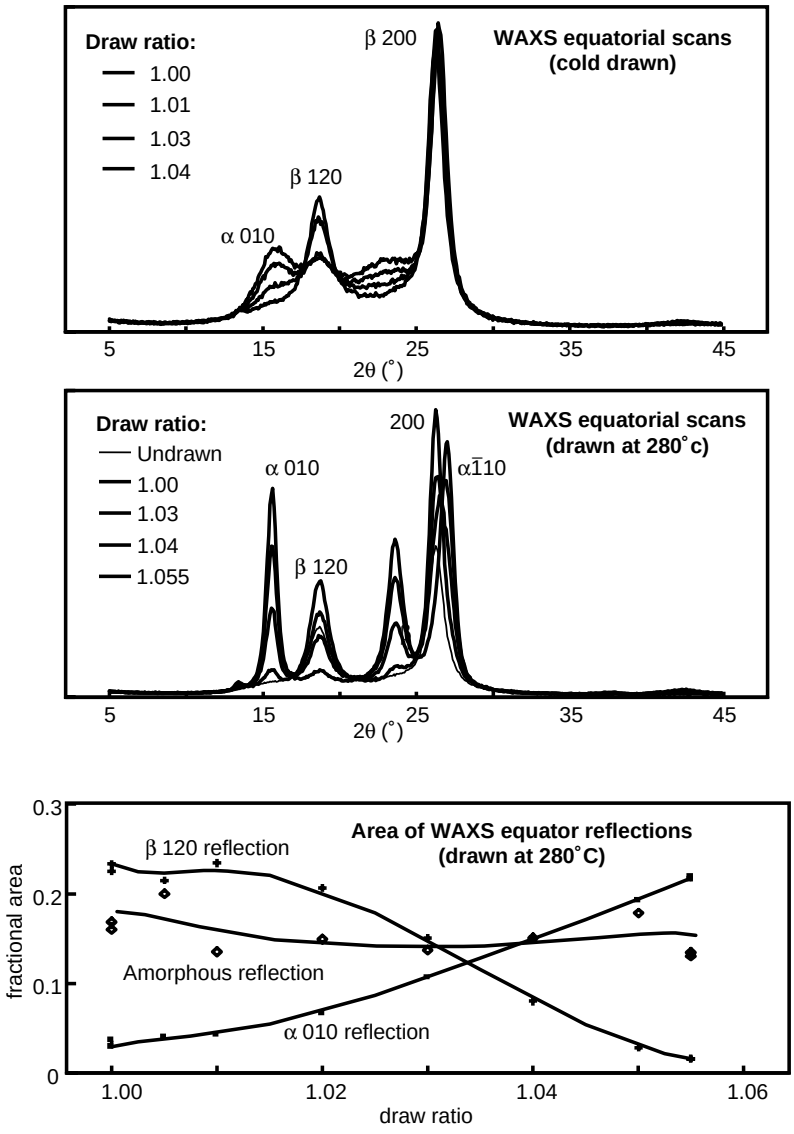

Fig. 8. Effect of drawing on the crystal structure of PEN-β yarns.

4.3. The effect of drawing on the physical structure and the shape of the stress–strain curve

The shape of the stress–strain curve of the PEN yarn spun at low draw-down, is typical of high-speed as-spun yarns (Fig. 7). The shape of the curve of the yarn spun at high draw-down is similar to that of a drawn yarn, apart from the unusual long yield area, ranging from about 2 to 5% elongation. A similar plateau has been observed in the case of poly(tetramethylene terephthalate), for which it marks the critical stress for transformation of α-crystals, containing crumpled molecular chains, to extended β-crystals. This transition, which consists of a conformational change of the glycol residue from the *gauche–trans–gauche* to the *trans–trans–trans* conformation, is reversible in general, and so is the stress–strain behavior [35–37]. In the subject case, the yield area marks the region where, at a stress of about 300 mN/tex, the sinusoidal chains within β-crystals transform into the extended chains of α-crystals. Just as for the polymorphic $\gamma \Rightarrow \alpha$ transition of crystals in high-speed spun polyamid 6 [38,39], the transition is not reversible and neither is the stress–strain behavior. So, after 3% drawing at room temperature, the WAXS equatorial β 120 reflection of high-speed spun PEN-β yarn, has diminished substantially in intensity (Fig. 8). Simultaneously, the intensity of the α-010 reflection increases, be it somewhat more gradually (see the picture at the top of Fig. 8, where the α 010 reflection still increases in intensity going from a draw ratio of 1.03 to 1.04, whereas the β 120 reflection hardly decreases). So, the $\beta \Rightarrow \alpha$ transition, which requires a 180° rotation of the rings in the β (200) planes, seems to proceed gradually. Remarkably, the width of the peak at $2\theta \approx 26.5°$ does not change much during this process.

If the drawing is carried out at 280°C, the $\beta \Rightarrow \alpha$ transition of crystals is much more straightforward (Fig. 8). Fig. 9 displays the mechanical properties of a yarn sample after

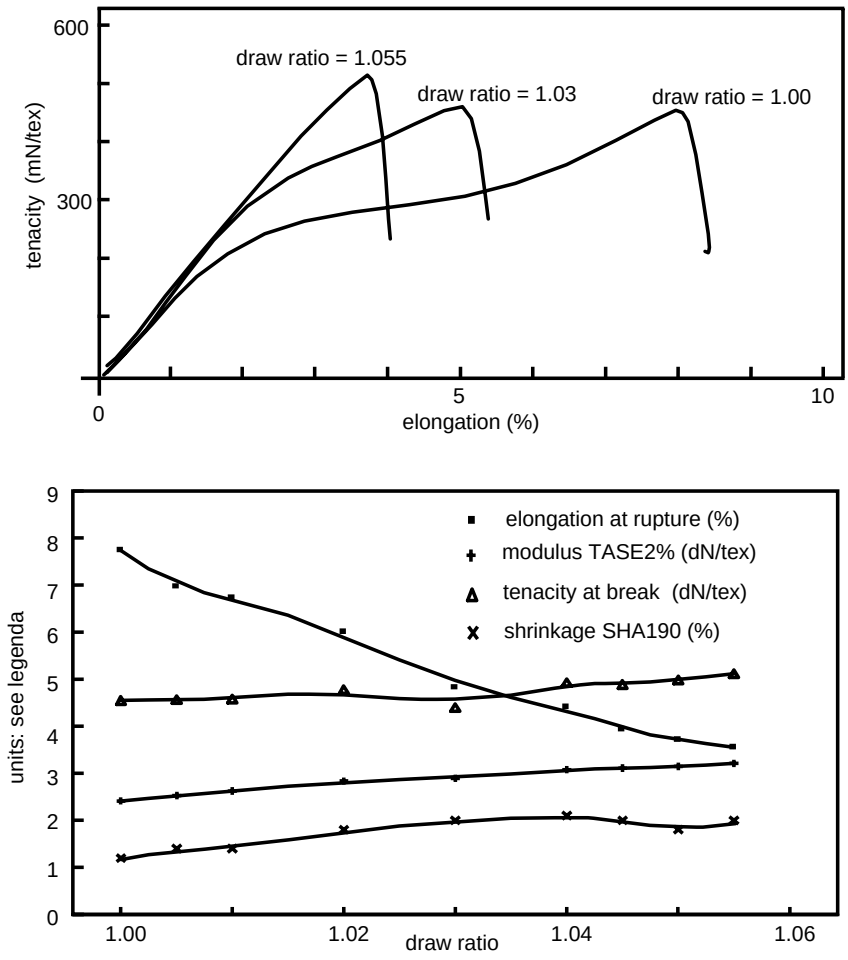

Fig. 9. Stress–strain curves and mechanical properties of PEN-β yarns after drawing at 280°C.

having been subjected to different draw ratios at 280°C. From the stress–strain curves, it can be concluded that the disappearance of the yield plateau with increasing draw ratio is a direct consequence of the β ⇒ α crystal transition. It is noted that the mechanical properties might be somewhat affected by mechanical damage of the low denier yarns during drawing on the simple drawing equipment.

The increase of extended α-conformations in the crystalline and amorphous regions on drawing gives rise to higher sonic moduli (Fig. 10). On the other hand, as the density of the α-polymorph is comparable to that of the β-polymorph, the density does not change substantially with the draw ratio (Fig. 10). On heating at 280°C, however, there is an incremental increase of both the sonic modulus and density which can be attributed to an increase of the crystallinity. As may be expected, the crystals after drawing at 280°C are thicker than those in yarns drawn at room temperature. Accordingly, their melting points are also slightly higher (Fig. 11). However, more interesting is that the melting point decreases only slightly with the draw ratio. It means that the melting point of α- and β-polymorphs are quite similar (note that at a draw ratio of 1 the yarn contains almost exclusively β-crystals and at a draw ratio of 1.055 mainly α-crystals). It can be concluded that the unusually high melting points hardly depend on the polymorphic form of the crystals but, as discussed above, must be due to orientation induced crystallization.

5. Thermal behavior of α- and β-crystals in PEN

Further insight into the thermal behavior of the α- and β-crystals was obtained by heating a yarn sample containing a mixture of both crystals. Equatorial WAXS scans were recorded at various temperatures (Fig. 12). Although the β $\bar{2}00$ reflection cannot be observed separately from the α $\bar{1}10$ reflection it is fair to conclude from Fig. 12 that the β 120 reflection sharpens considerably more than the β 200 reflection. This indicates that the apparent thickness of the β-crystals increases more strongly in the direction perpendicular to the (120) planes than in the direction perpendicular to the (200) planes. Fig. 13 shows a projection of the PEN-β structure along the *c*-axis in which all carbonyl–carbonyl contacts shorter than 5.0 Å are indicated. In view of the relatively short distances between the latter carbonyl groups, these contacts represent dipole–dipole interactions. A simple explanation of the sharpening of the β 120

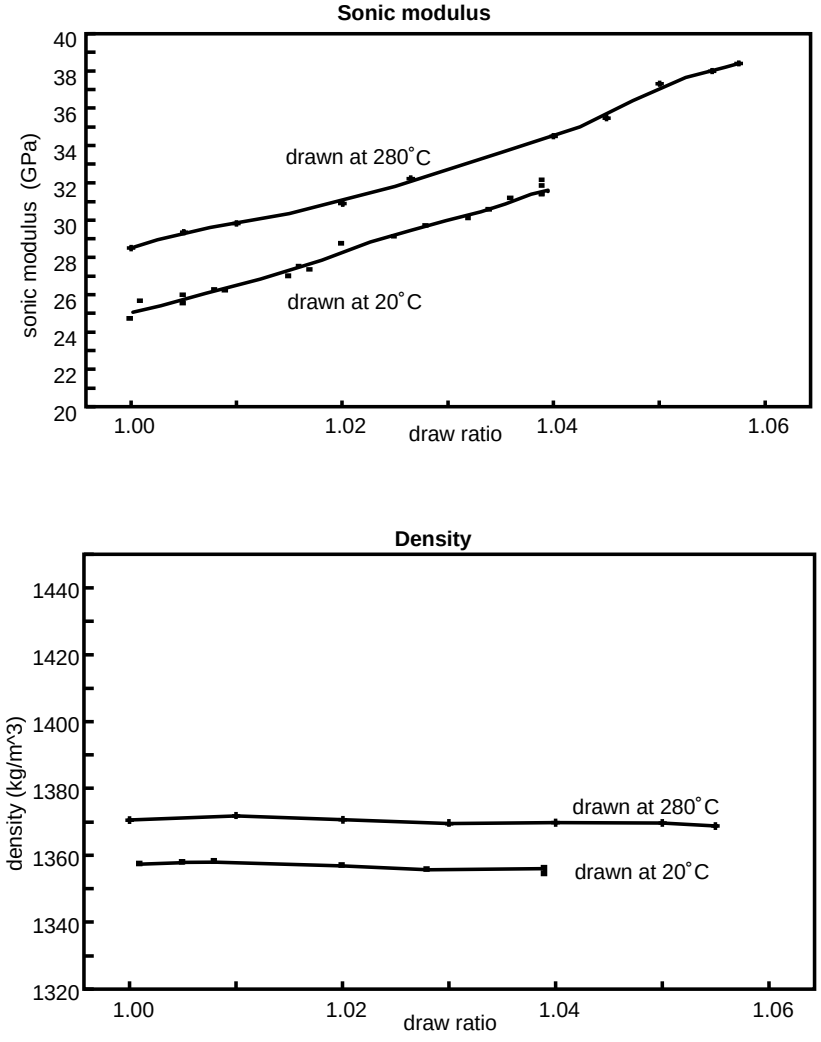

Fig. 10. Effect of drawing on the sonic modulus and density of PEN-β yarns.

reflection may be that the dipole–dipole interaction favors crystal growth along the (120) planes (and ($\bar{1}$20) planes) leading to lozenge-shaped crystals.

Fig. 12 shows that α-crystals melt at slightly lower temperatures than β-crystals, which is in line with the DSC results. No indications were found for thermally induced α ⇔ β crystal transitions. The shift of reflections towards lower diffraction angles indicates thermal expansion which takes place especially in the direction perpendicular to the aromatic rings (about 7% in the case of the β-crystals and about 5% in the case of the α-crystals). This can be explained by temperature induced rotation (libration) of the polymer chains around their axes.

6. Thermo-mechanical treatments during the production and processing of tyre yarns

When used for tyre reinforcement, yarns are subjected to rather complex processing steps such as conversion into cords by twisting and cabling followed by weaving to obtain a fabric. The fabric is dipped to provide it with a coating, which usually consists of a first layer with epoxide that adheres to the yarn surface. Subsequently, the main dip is applied, which is mostly based on a resorcinol fomaldehyde latex (rfl) that adheres to rubber. The dipping steps comprise extensive thermo-mechanical treatments with temperatures far above 200°C. After dipping, the fabric is coated on either side with a thin layer of rubber compound by means of calendering. During this step the fabric is heated and kept under tension to prevent relaxation. The rubberized fabric serves as carcass ply and is one of the many components from which the green tyre is assembled. Finally, during vulcanization (curing) of the tyre, the carcass cords shrink more or less freely (relaxation) at a temperature of about 180°C.

As a result of all these thermo-mechanical treatments, the physical structure of the yarns changes substantially. For

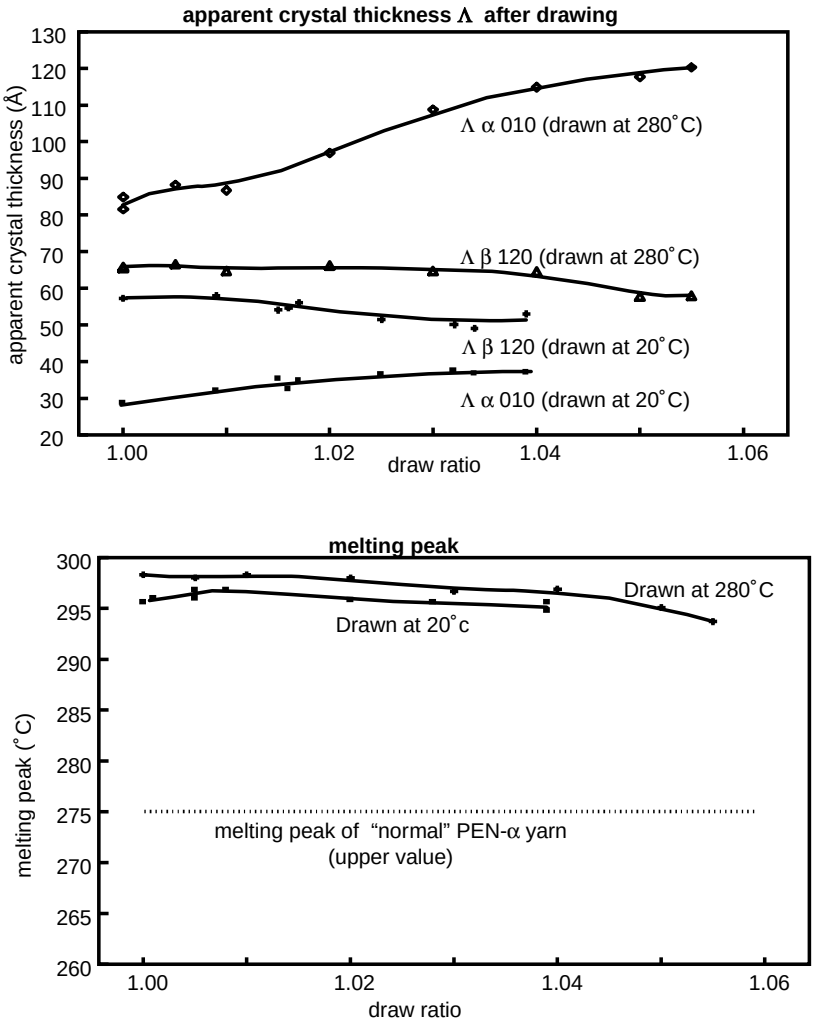

Fig. 11. Effect of drawing on the apparent crystal size and melting point of PEN-β yarns.

instance, in the case of the semi-crystalline PET and PEN yarns, the crystallinity may increase up to saturation, and during curing molecular coiling in the amorphous regions occurs. Also the mechanical properties change substantially. Therefore, in studying the suitability of yarns for tyre reinforcement, it is important to do so after a dip and cure simulation.

7. Mechanical properties of cords after dipping and curing

Typical tyre yarns (1100 dtex) made from PET (Diolen 1125T), PEN (low-speed spun with α-crystals and high-speed spun with β-crystals), rayon (Cordenka 700), and aramid (Twaron 1000), were converted into cords (two singles; twisting factor of about 175) and subjected to conditions typical of the hot-stretch dipping step. The applied heat treatments were in accordance with common practice, and, therefore, slightly different for the various samples. The cure simulation was carried out by heating the cords tensionless during 15 min at 165°C. Fig. 14 represents some cord properties after dip and cure simulation. As may be expected, aramid has the best performance in terms of breaking tenacity (BT) and modulus (TASE2%, i.e. tenacity at specific elongation of 2%). Furthermore, in comparison with rayon, the two PEN yarns perform well. Both their breaking tenacity and modulus are somewhat higher than that of rayon. So, at first glance, PEN seems to be a good alternative to rayon for tyre reinforcement. However, for tyre yarns also the dynamic response should be taken into account. This is considered in the next section.

8. Dynamic mechanical properties

Rotation of a tyre during driving results in periodic load cycles of the tyre cord with frequencies ranging from 0 to about 45 Hz for passenger car tyres (in the case of trucks up to 15 Hz). The frequency spectrum of such a loading pattern is very broad and therefore difficult to reproduce. We simulated the dynamic behavior by applying a 1 Hz sinusoidal

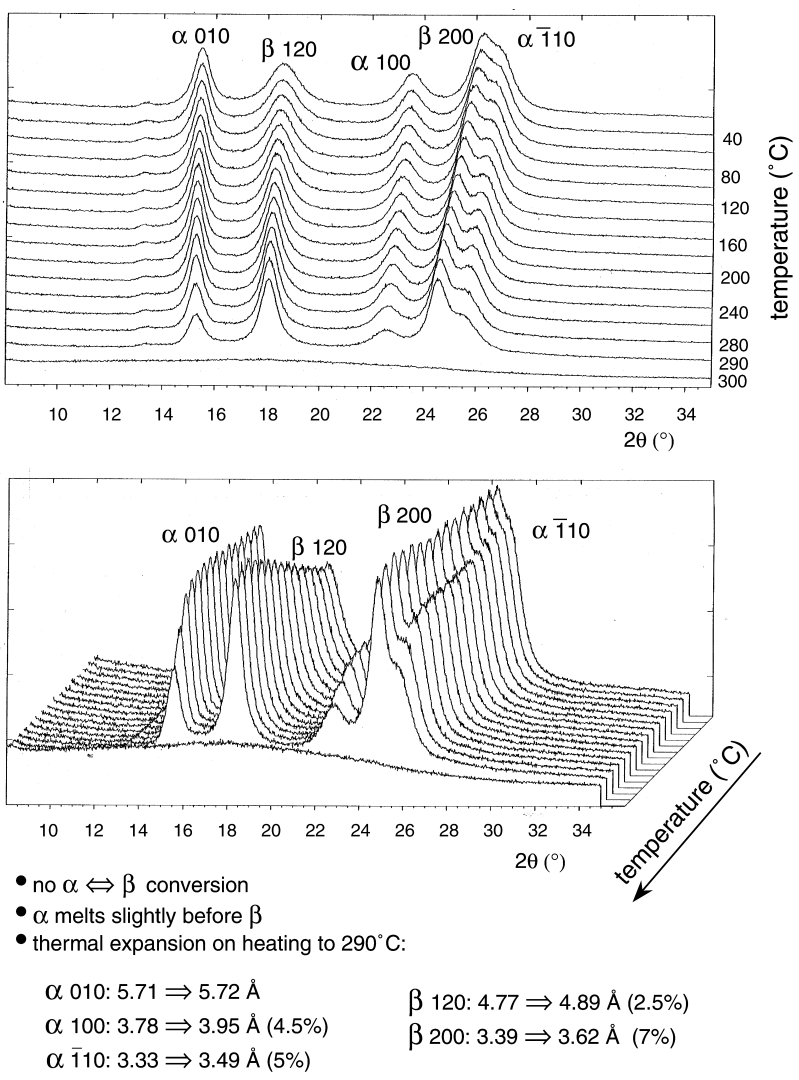

Fig. 12. PEN yarns containing α- and β-crystals: effect of temperature on equatorial WAXS scan.

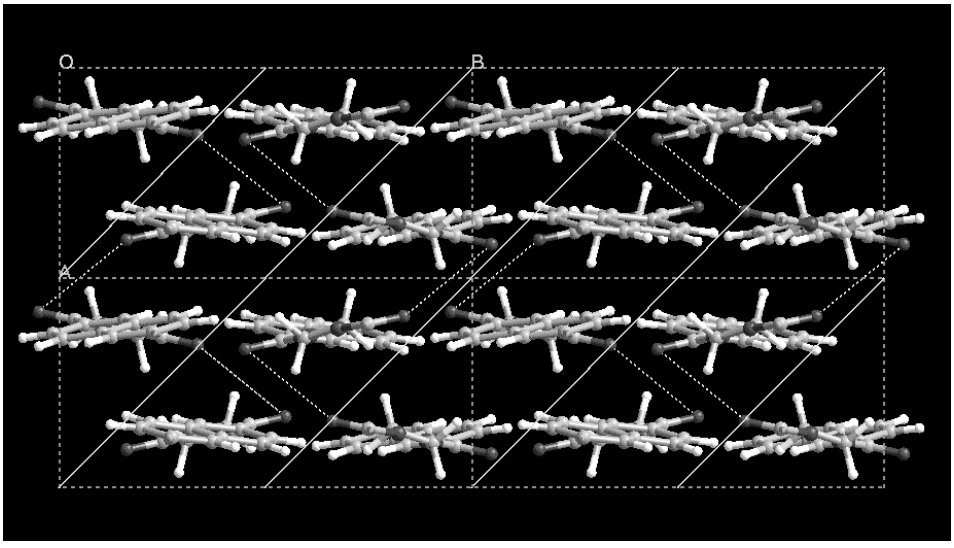

Fig. 13. Projection of the PEN-β crystal structure along the *c*-axis. Solid lines indicate (120) planes. Dashed lines between carbonyl groups indicate dipole–dipole interactions.

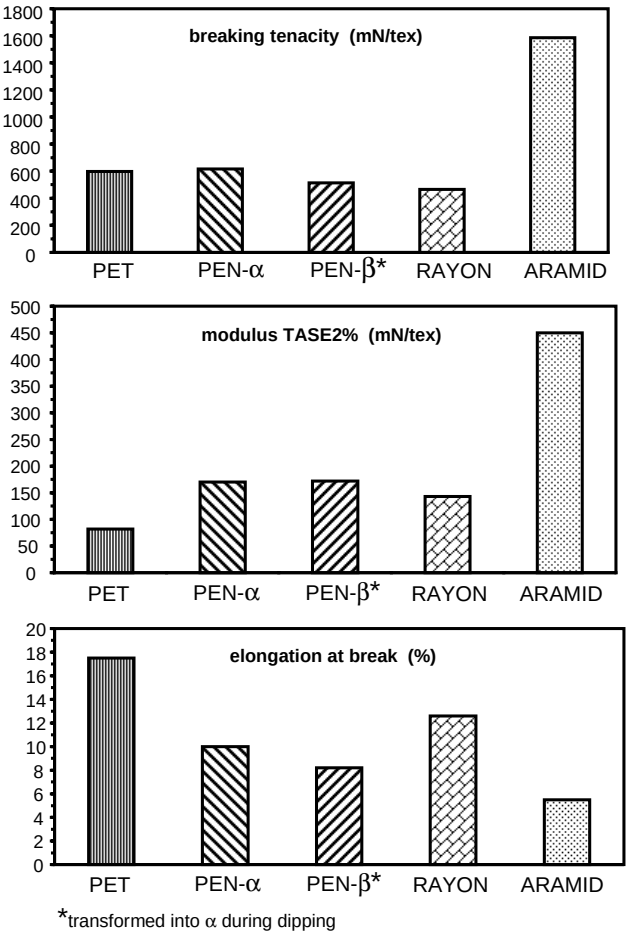

Fig. 14. Cord properties after dipping and curing.

stress at temperatures ranging from 20 to 200°C (in the shoulder of the truck tyres the temperature may reach values of over 130°C). Furthermore, it should be borne in mind that the polymer response to a 10 times higher frequency is roughly similar to the response at a 7°C lower temperature (superposition principle).

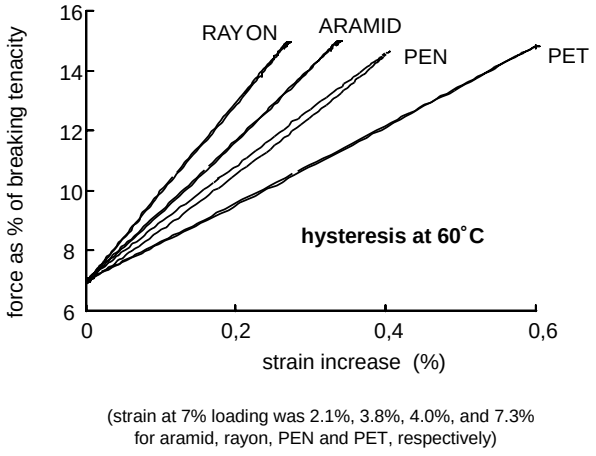

Fig. 15. Hysteresis curves of cured cords on dynamic loading between 7 and 15% of the breaking strength (1 Hz).

Beforehand, the cords were heat-treated as described in the previous section, except that the twisting factor was 205 and the curing was carried out at 180°C. The dynamic testing was done with intervals of 10°C starting at 20°C. At each temperature, the cords were subjected to a series of 100 cycles at various upper and lower load levels. The upper and lower load levels, simulate the inflation pressure and the resultant of inflation pressure and axle load, respectively. Details of these stress-controlled measurements are described elsewhere [25]. For calculating the dynamic response at each temperature, we used the 90th cycle between stress levels corresponding with 7 and 15% of the breaking strength of the cord. The applied load levels are realistic, taking into account that normalization to yarn strength is common practice in the tyre industry.

Fig. 15 represents the hysteresis loops as measured with a load-controlled frame at 60°C for high-speed spun PET Diolen 1125T, low-speed spun PEN-α, rayon Cordenka 700, and aramid Twaron 1000. From these curves the storage modulus E' was calculated, which is the part of the modulus that is in phase with the applied stress. The actual stiffness of a tyre during driving will substantially depend on the storage modulus E'. In Fig. 16, the storage modulus of the different cords is shown as a function of the temperature. At 20°C, the ranking of the modulus is similar to that of the static measurements. On a temperature increase the moduli decrease for two reasons. First of all, molecules become more separated because of thermal expansion, which causes a reduction of the intermolecular interactions. The decrease is roughly 0.1%/°C, which is in line with the literature values [40]. Another reason for the decrease in modulus with temperature is the occurrence of relaxation processes. In the case of the semi-crystalline PET and PEN yarns, the most important relaxation process is the glass rubber transition that occurs when the temperature has reached values at which molecules in the amorphous regions no longer have fixed positions. This leads to a substantial decrease of the storage modulus. For PET and PEN the glass transition temperatures are about 80 and 125°C, respectively. The higher glass transition in the case of PEN reflects the higher stiffness of its molecular chains. In the case of PEN, there is also a relatively fast decrease of E' around 60°C, which is a normal running temperature for passenger car tyres. This phenomenon becomes even more salient when the moduli are scaled relative to their value at 20°C. From Fig. 16, it follows that the reduction of the modulus is about 20% going from 20 to 60°C. Therefore, it is likely that tyres reinforced with PEN may have a more than usual reduction of stiffness when they warm up during driving, which may influence the steering behavior of the car.

Another aspect of PEN to be mentioned here is the banana shape of its hysteresis (Fig. 15), which shows that the work loss during dynamic loading is high when compared with other yarns (the work loss corresponds with the area of the banana). Fig. 17 shows the work loss of the different yarns as a function of temperature. What is striking is the large

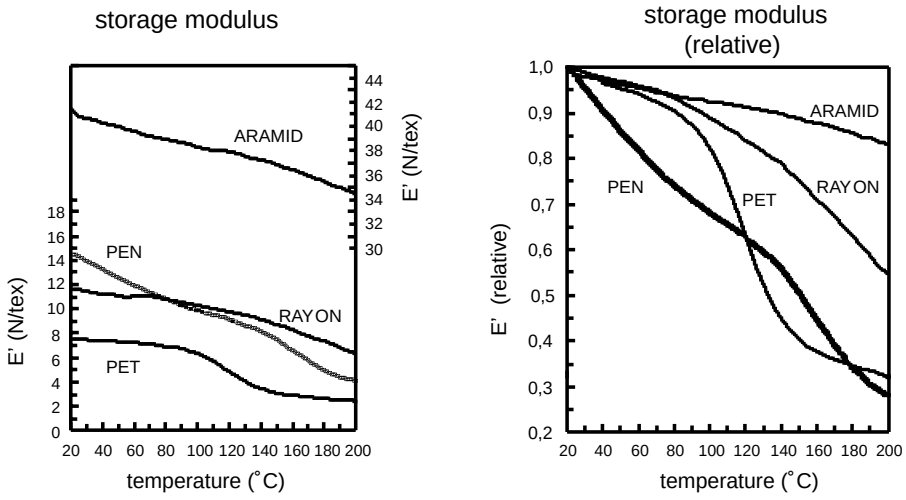

Fig. 16. Storage modulus of cured cords on dynamic loading between 7 and 15% of the breaking tenacity (1 Hz).

work loss of PEN over the whole temperature range. After scaling to strength, which is the prime parameter for tyre yarns, the differences are even more pronounced: at moderate in-use temperatures, the work loss of PEN is four times higher than that of the other reinforcement materials. Taking into account that the reinforcement material may contribute substantially to the heat generation of the tyre [25], it seems that the higher work loss may lead to higher fuel consumption during driving.

We also studied the dynamic behavior of steam-drawn PET and PEN yarns by strain controlled dynamic mechanical analysis (DMA) at temperatures between −150 and

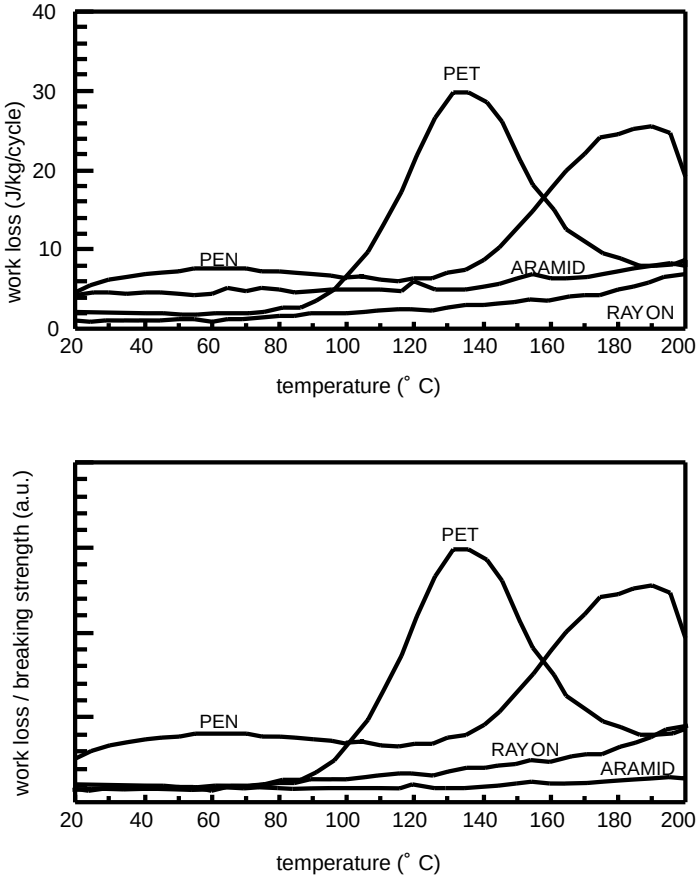

Fig. 17. Work loss of cured cords on dynamic loading between 7 and 15% of the breaking strength (1 Hz).

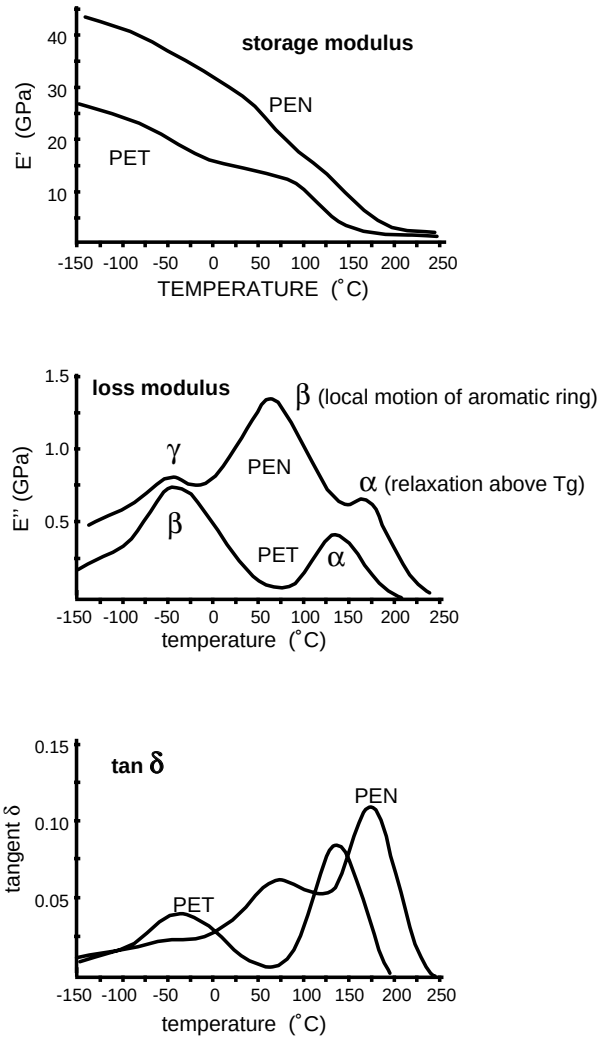

Fig. 18. Dynamic Mechanical Analysis of PEN and PET yarns (10 Hz).

250°C, applying a frequency of 10 Hz, which roughly corresponds with that of the cyclic deformation of a car tyre at a driving speed of 70 km/h. The measurements were carried out on greige yarns imposing a static strain of 0.5% and a dynamic strain of 0.05%.

The change in modulus with temperature, as measured for PET and PEN yarns with strain controlled DMA measurements (Fig. 18), corresponds quite well with that observed with the load controlled measurements on cords in the overlapping temperature range (Fig. 16), despite the differences in loading, cycle frequencies, sample preparation, and so on. From Fig. 18 it is clear that the decline of the elastic, in phase part of the modulus, E', is larger for PEN than for PET over the entire temperature range. The corresponding curve of the loss modulus E'', i.e. the viscous part of the modulus which is out of phase with the applied strain, shows several peaks that mark temperatures at which the frequency of specific molecular relaxation processes equals the imposed cycle frequency of 10 Hz. Actually, E'' is a measure of the energy, that is lost as heat, due to the molecular transitions occurring with each cycle. In Fig. 18, there is also a plot of the ratio of E'' and E', i.e. of tan δ, where δ is the angle between the in-phase and out-of-phase components in the cyclic motion. Following convention, the relaxations are labeled α, β, and γ, in order of decreasing peak temperature. The α-relaxations mark the glass–rubber transition. The β-relaxation of PET and the γ-relaxation of PEN at about −50°C are generally attributed to local motions of methylene groups and, in the case of PET, also to motions of the phenyl ring [40,41]. The peak at about 60°C is characteristic of polymers that contain naphthalene rings and arises from motions of these rings (below T_g), irrespective of whether they are attached to ester carbonyl groups or not [41]. Further, the motions are considered to consist of essentially full rotation of the rings. The average number of transitions per second is given by $\nu^* = \nu_0 \exp[-\Delta H/RT]$, in which ν_0, the vibration frequency in the potential well, is about 10^{13} Hz, $\nu^* = 10$ or 1 Hz, and R is the gas constant (2×10^{-3} kcal/mol °C) [40]. So, the activation energy is about 18 kcal/mol, which is considerably higher than the 12 kcal/mol required for the rotation of phenyl rings. The higher activation energy can be attributed to the absence of a rotation axis through the $C_{aliphatic-Caromatic}$ bonds of the naphthalene ring, as a result of which rotation is hindered as it requires synchronous conformational changes of neighboring parts of the molecular chain.

Considering the three conformations of the naphthalene ring, i.e. *trans*-α, *trans*-β and *cis* (Fig. 1), one may question which conformational changes are most likely. To this end, we calculated the energies for the α ⇔ β, α ⇔ *cis*, β ⇔ *cis* and *cis* ⇔ *cis* transitions with Insight/Discover on the dimethyl ester of naphthalenedicarboxylic acid (Fig. 19). It turns out that the activation energies for all four transitions between the three conformations are about 6 kcal/mol (the energy for rotation of a phenyl group is about 5 kcal/mol). The fact that this value of 6 kcal/mol is much lower than the actual 18 kcal/mol for rotation of the naphthalene ring in PEN, points to the strong molecular interactions attending the rotation. On closer examination of the molecular conformations (cf. Fig. 1), it appears that the α ⇔ *cis* and β ⇔ *cis* transitions call for very large conformational changes of neighboring monomer units in the polymer chain. Below T_g, these changes are unlikely. Therefore, the ring rotations at 60°C can best be associated with α ⇔ *β* and *cis* ⇔ *cis* transitions, although even then conformational adjustments of neighboring monomer units are necessary. Such adjustments are not necessary for rotation of the phenyl ring in PET, as finds expression in its lower activation energy of rotation (12 kcal/mol).

9. Conclusions

Semi-crystalline PEN yarns can be produced by a simple one-step melt spinning process. The yarns contain

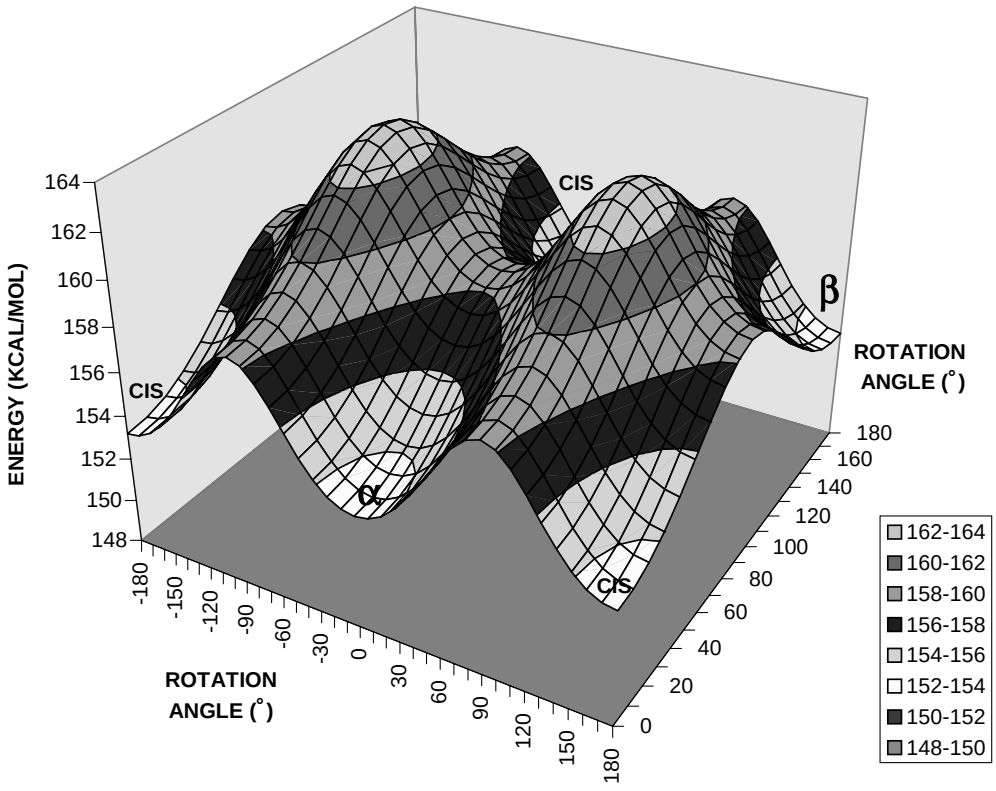

Fig. 19. Conformational energies on rotating the naphthalene ring around the ester groups in the dimethyl ester of naphthalenedicarboxylic acid.

β-crystals in which polymer chains have a sinusoidal conformation. Under the influence of stress the crystals transform irreversibly into the fully extended α-form by rotation of the naphthalene rings. Although PEN yarns combine a good breaking tenacity with a high modulus, rotation of the naphthalene rings in the amorphous domains brings about a more than usual decrease of the dynamic modulus with the temperature, and gives rise to a high work loss.

Acknowledgements

The authors wish to thank D.B. van Guldener and J. Jager for preparing the PEN polymer, H. Middeljans, L.A.G. Busscher and J.A. Juijn for spinning the fibers, E.A. Sjerps-Koomen for studying the drawing of PEN, E. Th. Steyn, F. Elkink, A.J. de Vries and H.J. Hermann for analyzing the mechanical properties of the yarns and cords, and J. Aerts for performing the conformational energy calculations.

References

[1] Patent US 4000239 in the name of Teijin Limited.
[2] Mencik Z. Chem Prum 1976;17:78.
[3] Jackson WJ. Macromolecules 1983;16:1029.
[4] Zachmann HG, Wiswe D, Gehrke R, Riekel C. Makromol Chem, Suppl 1985;12:175.
[5] Cheng SZD, Wunderlich B. Thermochim Acta 1988;134:161.
[6] Cheng SZD, Janimak JJ, Zhang A, Guan J, Chu A-L. Polym Bull 1988;20:449.
[7] Cheng SZD, Wunderlich B. Macromolecules 1988;21:789.
[8] Cheng SZD, Wunderlich B. Thermochim Acta 1988;134:161.
[9] Cheng SZD, Pan R, Bu HS, Cao M-Y, Wunderlich B. Makromol Chem 1988;189:1579.
[10] Cheng SZD, Janimak JJ, Zhang A, Guan J, Chu A-L. Polym Bull 1988;20:449.
[11] Buchner S, Wiswe D, Zachmann HG. Polymer 1989;30:480.
[12] Cakmak M, Wang YD. Simhambhatla. Polym Engng Sci 1990;30:721.
[13] Nakamae K, Nishino T, Tada K, Kanamoto T, Ito M. Polymer 1993;34:3322.
[14] Huijts RA, Peters SM. Polymer 1994;35:3119.
[15] Nakamae K, Nishino T, Gotoh Y. Polymer 1995;36:1401.
[16] Abis L, Merlo E, Po R. J Polym Sci Part B: Polym Phys 1995;33:691.
[17] Jager J, Juijn JA, van den Heuvel CJM, Huijts RA. J Appl Polym Sci 1995;57:1429.
[18] Jakeways R, Klein JL, Ward IM. Polymer 1996;37:3761.
[19] Marakami S, Yamakawa M, Tsuji M, Kohjiya S. Polymer 1996;37:3945.
[20] Cakmak M, Kim JC. J Appl Polym Sci 1997;64:729.
[21] Miyata K, Kikutani T, Okui N. J Appl Polym Sci 1997;65:1415.
[22] Baltá Calleja FJ, Rueda DR, Michler GH, Naumann I. J Macromol Sci Phys 1998;37(4):411–9.
[23] Lee SW, Cakmak M. J Macromol Sci Phys 1998;B37(4):501–26.
[24] Patents US 5466525 and US 5618480 in the name of Akzo Nobel N.V.
[25] Otto MJ, Steyn ETh, Elkink F. Kautsch Gummi Kunstst 1997;50:192.
[26] Heuvel HM, Huisman R. J Appl Polym Sci 1989;37:596.

[27] Insight/Discover, V.3.0.0, BiosymTechnologies Inc., San Diego, 1995.
[28] Northolt MG, van den Hout R. Polymer 1985;26:310.
[29] Klop EA, van den Heuvel CJM, in preparation.
[30] Liu J, Sidoto G, Hommema JA, Geil PH, Kim JC, Cakmak M. J Macromol Sci Phys 1998;B37(4):567–86.
[31] Heuvel HM, Huisman R. J Appl Polym Sci 1978;22:2229.
[32] Ziabicki A. In: Ziabicki A, Kawai H, editors. High speed fiber spinning, New York: Wiley, 1985 part 1, chap. 1.
[33] van den Heuvel CJM, unpublished results.
[34] Ziabicki A. In: Ziabicki A, Kawai H, editors. High speed fiber spinning, New York: Wiley, 1990 part 1, chap. 2.
[35] Jakeways R, Smith T, Ward IM, Wilding MA. J Polym Sci (Polym, Phys Ed) 1976;14:41.
[36] Roebuck J, Jakeways R, Ward IM. Polymer 1992;33:227.
[37] Nitzsche SA, Wang YK, Hsu SL. Macromolecules 1992;25:2397.
[38] Heuvel HM, Huisman R, Ziabicki A, Kawai H. High speed fiber spinning. Wiley: New York, part 3, chap. 11.
[39] Shimizu J, Okui N, Kikutani T, Ono A, Takaku A. Sen-i Gakkaishi 1981;37:143.
[40] Struik LCE. Internal stresses, dimensional instabilities and molecular orientations in plastics, New York: Wiley, 1990 ISBN 0471-92642-6.
[41] Ward IM. Makromol Chem, Macromol Symp 1993;69:75.